iPSC-Neural Crest Derived Cells Embedded in 3D Printable Bio-Ink Promote Cranial Bone Defect Repair

Juliane D Glaeser
Cedars-Sinai Medical Center
Xianchao Bao
Cedars-Sinai Medical Center
Giselle Kaneda (giselle.kaneda@cshs.org)
Cedars-Sinai Medical Center
Pablo Avalos
Cedars-Sinai Medical Center
Phillip Behrens
Cedars-Sinai Medical Center
Khosrowdad Salehi
Cedars-Sinai Medical Center
Xiaoyu Da
Cedars-Sinai Medical Center
Angel Chen
Cedars-Sinai Medical Center
Wensen Jiang
Cedars-Sinai Medical Center
Chloe Castaneda
Cedars-Sinai Medical Center
Wafa Tawackoli
Cedars-Sinai Medical Center
Dmitriy Sheyn
Cedars-Sinai Medical Center https://orcid.org/0000-0002-3333-1485

Research Article

Keywords: Cranial repair, 3D Printing, neural crest cells, iPSC, bone healing

Posted Date: May 6th, 2022

DOI: https://doi.org/10.21203/rs.3.rs-1562664/v1

Abstract

Background

Cranial bone loss presents a major clinical challenge and new regenerative approaches to address craniofacial reconstruction are in great demand. Induced pluripotent stem cell (iPSC) differentiation is a powerful tool to generate mesenchymal stem cells (MSCs). Prior research demonstrated the potential of bone marrow-derived MSCs (BM-MSCs) and iPSC-dervied mesenchymal progenitor cells via the neural crest (NCC-MPCs) or mesodermal lineages (iMSCs) to be a promising cell source for bone regeneration. Overexpression of human recombinant bone morphogenetic protein (BMP)6 efficiently stimulates bone formation. The goal of this study was to evaluate the potential of iPSC-derived stem cells via neural crest or mesoderm overexpressing BMP6 and embedded in 3D printable bio-ink to generate viable bone graft alternatives for cranial reconstruction.

Methods

Cell viability and osteogenic potential of cells and bio-ink (Ink-Bone or GelXa) combinations were investigated in vitro using bioluminescent imaging. Osteogenic potential of bio-ink-cell constructs was evaluated in osteogenic media or nucleofected with BMP6 using qRT-PCR and in vitro µCT. For *in vivo* testing, two 2mm circular defects were created in the frontal and parietal bones of NOD/SCID mice and treated with Ink-Bone, Ink-Bone + BM-MSC-BMP6, Ink-Bone + iMSC-BMP6 or Ink-Bone + iNCC-MPC-BMP6 or left untreated. For follow up, µCT was performed at weeks 0, 4 and 8 weeks. At time of (week 8), histological and immunofluorescent analyses were performed.

Results

Both bio-inks supported cell survival and promoted osteogenic differentiation of iNCC-MPCs and BM-MSCs in vitro. At 4 weeks, cell viability of both BM-MSCs and iNCC-MPCs were increased in Ink-Bone compared to GelXA. Combination of Ink-Bone with iNCC-MPC-BMP6 resulted in an increased bone volume in the frontal bone compared to the other groups at 4 weeks post-surgery. At 8 weeks, both iNCC-MPC-BMP6 and iMSC-MSC-BMP6 resulted in an increased bone volume and partial bone bridging between implant and host bone compared to the other groups.

Conclusions

The results of this study show the potential of NCC-MPC-incorporated bio-ink to regenerate frontal cranial defects. Therefore, this bio-ink-cell combination should be further investigated for its therapeutic potential in large animal models with larger cranial defects, allowing for 3D printing of the cell-incorporated material.

Introduction

In cases of extreme bone loss following a traumatic injury, in which the mechanism of bone self-repair is inadequate, grafts or alloplastic materials are typically used to repair the defect. The current market value for craniofacial bone replacement is estimated to be $390 million for trauma alone, representing 13% of all traumatic bone injuries [1]. The “gold standard” for stimulation of new bone formation is autologous bone grafting [2]. However, donor-site morbidity is a limiting factor [3]. Cranioplasty with alloplastic materials like Titanium or polymers like polymethyl methacrylate and polyether ether ketone are often associated with high rates of infection and complications [3]. The introduction of three-dimensional computed tomography has revolutionized calvarial reconstruction through the creation of anatomic alloplastic models [4]. However, these models typically need to be combined with autografts. Furthermore, alloplastic materials are also not ideal for use in children and juveniles due to cranial growth. Recombinant osteogenic growth factors, such as recombinant human bone morphogenetic proteins (rhBMP), are only used to treat small bone lesions due to their high cost and safety concerns including inflammation and swelling [1, 5].

3D bioprinting is a developing technology that can create scaffolds from different biomaterials that precisely mimic the shape, size, and dimension of a defect [6]. Although many 3D bioprinting methods, including those used in dentistry, produce constructs with suitable interconnected porosity and mechanical properties, they often require the application of high temperatures, solvents, or other conditions that are not compatible with living cells [7]. Post-production seeding of cells has been reported to result in a non-uniform cell distribution and poor cell attachment [8]. A potential solution to include cells in 3D printing is the use of soft bio-inks that are crosslinked post-production. These bio-inks can be synthetic or natural polymers [9–11]. A perfect bio-ink should be printable into different structures, mechanically stable, cytocompatible, and non-immunogenic and have a suitable degradation rate [12]. One option is to use alginate, an inexpensive biomaterial that has been widely studied for diverse biomedical applications including cartilage and bone [10, 13], due to its excellent cell responses and flexible gelation preparation through divalent ions including calcium.

Bone marrow-derived Mesenchymal Stromal Cells (BM-MSCs) are the most utilized cells for long bone regeneration due to their accessibility [14–16]. However, the use of BM-MSCs did not support the repair of large cranial defects without viral transduction with rhBMP-2 [17]. Reasons for these outcomes might be the different bone structures and cellular content of craniofacial and long bones. Craniofacial bones are flat, formed through intramembranous ossification, and develop from embryological origins distinct from those of long bones [18]. Within the cranium, only the parietal bones are of mesodermal origin, whereas the formation of frontal cartilage and bone originates in the neural crest (NC) [19, 20]. Interestingly, a higher regeneration potential has been shown in NC-derived compared to mesoderm-derived calvarial bones [21]. Furthermore, cells obtained from NC bone were shown to be more osteogenic, more proliferative, and less apoptotic [22–24]. During embryogenesis, neural crest cells (NCCs) are identified within the dorsal margins of the closing neural fold [25], then migrate into various skeletal tissues [26]. Their profound role in cranial skeletogenesis makes NCCs an attractive cell source for cranial repair.

Although this cell type is rare in adults, it can be obtained through the induced pluripotent stem cell (iPSC) differentiation [27–29]. Our prior study demonstrates that iPSC-derived NC mesenchymal progenitor cells (iNCC-MPC) are more efficient in revitalizing cranial allografts than BM-MSCs.[30] Since cell source and mode of differentiation both may affect the cells' performance, a direct comparison between iNCC-MPCs and iMSCs should be performed [30].

The BMP family and its 20 identified members play an important role in osteogenesis [31, 32]. Adenovirus-mediated MSC transduction with 14 different human isoforms of BMP revealed that BMP2, BMP6, and BMP9 are the most potent inducers of osteogenesis in MSCs [33, 34]. Although less popular than BMP2, BMP6 overexpression in BM-MSCs or adipose-derived stem cells was demonstrated to be more potent in term of stimulation of bone formation [35].

In the present study, we hypothesize that iNCC-MPCs overexpressing BMP6 will induce bone formation in 3D printable bio-ink constructs and will regenerate cranial defects more efficiently in the frontal bone compared to mesodermal BM-MSCs and iMSCs.

The following aims were pursued: 1) In vitro investigation of different bio-ink – cell combinations to identify the ink that supports cell viability and osteogenic differentiation. 2) In vivo analysis of the critical defect healing potential of bio-ink in combination with BMP6 transfected BM-MSCs, iMSCs and iNCC-MPCs.

Methods

Experimental Design

Two types of bio-inks, CELLINK BONE (hereafter referred to in short Ink-Bone) or GelXA BONE (in short GelXA, both CELLINK Life Sciences, Boston, MA), were investigated in this study. For *in vitro* analysis, the cell viability and osteogenic potential of BM-MSCs and iNCC-MPCs was investigated when combined with the bio-inks. For cell viability testing, bioluminescent imaging (BLI) was performed for a duration of 4 weeks. For cell visualization, cells were transfected with a luciferase reporter gene prior to testing. For testing of the osteogenic differentiation potential, cells combined with each of the bio-ink types were either exposed to osteogenic media for a duration of 8 weeks or nucleofected with rhBMP6 (or GFP control) prior to bio-ink exposure. At week 8, RNA was isolated from the cell bio-ink constructs and qPCR analysis conducted using osteogenic primers. For *in vivo* testing, two 2mm circular defects were created in the frontal and parietal bone of NOD/SCID mice (n=39) were generated. Each defect was treated as follows: A) untreated (n=5), B) with Ink-bone only (n=8), C) with Ink-Bone + BM-MSC-BMP6 (n=5), D) with Ink-Bone + iMSC-BMP6 (n=7) or E) with Ink-Bone + iNCC-MPC-BMP6 (n=14). For follow up, µCT was performed at weeks 0, 4 and 8 weeks. At time of sacrifice (week 8), histological and immunofluorescent analyses were performed.

Cell derivation, culture and Luciferase transduction

Human BM-MSCs were isolated from whole bone marrow aspirate (Lonza, USA), using standard method and plastic adherence, as previously described [36]. Induced MSCs were differentiated from iPSCs, as previously published by our group [37]. Neural crest cells were differentiated from iPSCs and then further differentiated to iNCC-MPCs, as previously described [28, 29]. For investigation of cell viability in vitro, BM-MSCs and iNCC-MPCs were transduced with a lentiviral vector harboring the reporter gene luciferase2 (Luc2) under the constitutive ubiquitin promoter to allow in vivo imaging of cell survival, as previously reported [38, 39].

Preparation of cell-seeded bio-inks, 3D printing and Scanning Electron Microscopy

Two types of bio-inks, Ink-Bone or GelXA were combined with either BM-MSCs or NCC-MPCs derived from induced pluripotent stem cells (iNCC-MPCs) in a 9:1 ratio (bio-ink:cells). Briefly cells were lifted with 0.25% trypsin after washing with PBS, counted, and stained with DiI (Invitrogen, Carlsbad, CA) in PBS for 20 minutes. Cells were washed twice with PBS and pelleted. 900ml of CELLINK BONE or GelXA was combined with 10 million either BM-MSC-BMP6, iNCC-MPC-BMP6 or iMSC-BMP6 cells resuspended in 100µl 1XPBS (GIBCO, Waltham, MA), to achive 1:9 cells to bio-ink ratio. The bone-graft/cell combination was then transferred to a 3ml syringe. A leur lock adaptor was used to connect to another 3ml syringe and mix between the two syringes until the cell suspension was homogeneous.

The 3D printing was performed using a Cellink Bio X^{TM} 3D bioprinter. The construct design is a 10 mm x 10 mm x 2 mm squanre. Cells were pre-cultured to confluency and pre-mixed with the cellink bone using the recommended protocols from Cellink. The constructs were printed at 25-30kpa at 9m/ml concentration. The printhead is a 22-G plastic needle and the print speed is 10 mm/s. For samples used for SEM imaging, a 25-G plastic needle was used. The constructs were printed into a petridish. The petridish was then removed from the printer, and a Ca^{2+} crosslinking agent from Cellink was used to crosslink and solidify the construct.

The printed construct was frozen in liquid nitrogen before cross-sectional cutting and freeze-dried. Before imaging, samples were sputtered with gold using an SC7620 Polaron mini sputter coater (Quorum Technologies Ltd., Ashford, UK). Filament morphology and cross-section were assessed with the scanning electron microscope (SEM JEOL JSM-6390LV) (JEOL, Tokyo, Japan).

Bioluminescence imaging

To measure the viability of the cells seeded on the bio-inks, Luc2 expression was quantified using Bioluminescence Imaging (BLI) at days 1, 4, 7, 10, 14, 21 and 28, as described previously [38-40]. The IVIS camera image capture was set starting from 8-10 minutes after D-luciferin injection for peak BLI with a target max count (3,000 or 30,000 photon counts) and auto-exposure time (with a maximum exposure time of 1 minute) were set before acquiring the images. A circular Regions of interest (ROI) with 7-mm in diameter were applied to all acquired images to measure total flux (photons per sec) in ROI. Image acquisition and analysis were performed with Living Image software packages (Version 4.5.5). The image analysis was done using total influx data calculated from same size ROI (one well),

normalized to the background noise of each image. BLI signals were normalized to signals detected on day 1.

Cell nucleofection with BMP6

For cell nucleofection, the Amaxa Human MSC Nucleofector Kit was used (Lonza, Basel, Switzerland). Cells were washed with PBS (GIBCO) then lifted with 0.25% Trypsin-EDTA (Sigma, St Louis, MO) and counted and aliquoted at $1x10^6$ cells per 15ml conical tube. 2mL of DMEM (GIBCO) with 20% FBS was placed in 6-well plates and prewarmed in the 37°C incubator. Cells were resuspended in 100ml nucleofection solution (Lonza) and 10mg of BMP-6 plasmid was added to the solution and placed in a cuvette. The cuvette was placed in the Nucleofector II device (Lonza) and set to program G-22. After nucleofection, cells were immediately pipetted out of the cuvette and into the 6-well plate with prewarmed media. The final concentration in each well was 2×10^6 cells. The next morning the cells were lifted as described above, counted, and used for preparation of cell-seeded bio-inks.

Differentiation and qPCR testing

For testing of the osteogenic differentiation potential, both bio-inks were either combined with BMP6 (GFP control) nucleofected cells or non-transfected cells that were then exposed to osteogenic media for a duration of 8 weeks (or GFP control). The osteogenic media contained 0.1μM Dexamethasone, 10mM b-glycophosphate, 50μg/ml L-Ascorbic acid, as previously described [30, 41-43]. The cells' differentiation potential was confirmed at week 8 by osteogenic gene marker expression. RNA was isolated from the cell bio-ink constructs, transcribed into cDNA and qPCR analysis conducted, as previously described [30, 35, 41, 44, 45]. Taqman Gene Expression Assay for: osteocalcin (Oc), collagen type I (Col I), alkaline phosphatase (ALP) and osteonectin (On) were used for analysis.

Calvarial surgery

Animal surgeries were performed in accordance with the approved IACUC protocol #007961, as previously reported [46]. To create calvarial defects, the 8-week-old NOD/SCID mice were anesthetized with 2-3% isoflurane, and buprenorphine (0.05mg/kg) was injected subcutaneously (SQ) for analgesia. Animals were given thermal support for the duration of the procedure. The surgical site was shaved and aseptically prepped by thoroughly disinfecting with betadine and 70% isopropyl alcohol. Animals were placed on a stereotaxic instrument, with the skull secured with ear bars and a tooth bar. A straight incision (~15mm) was made over the midline to expose the parietal and frontal bones. Two 2 mm-diameter full-thickness circular skull defects, one in the parietal bone (alternating left and right of midline suture) and one in the frontal bone (alternating left and right of midline suture, opposite side to the parietal bone defect), were made using a Dremel drill. The drilling angle form midline suture was between 1-2mm to the left and right, respectively. Each defect was treated according to the experimental design. For defect filling, 10ml of Ink-Bone suspension with or without cells (measured with a 250ml Hamilton) was added per defect area via wax spatula followed by addition of a single drop of Crosslinking Agent (Cellink Life Sciences) for 30 seconds. Afterwards, the agent was carefully removed with a sterile gauze.

The skin incision was sutured using monofilament nylon non-absorbable suture (5-0 Ethilon black) in a horizontal mattress pattern. The animals were then removed from the stereotaxic instrument and given 1 ml of 0.9% saline SQ. A dose of buprenorphine (0.05mg/kg, SQ) was given on day 1 post-surgery and as needed thereafter. The antibiotic enrofloxacin was given daily for 5 consecutive days (5mg/kg; 0.06ml; SQ injection) to prevent infection. Sutures were removed 5 days after completion of the surgery. Mice were housed in groups of 5 for the whole study duration.

In vivo µCT analysis

Bone formation was monitored by µCT analysis in vivo, as previously described [47-49]. The mice were scanned post-surgery using a Viva CT 40 (Scanco Medical, Wangen-Brüttisellen, Switzerland) at day 1, week 4, and 8. Bone volume (BV), bone mineral density, connectivity density[50] were evaluated, as previously described [38, 47].

The mice were placed inside an induction chamber and anesthetized using a 4% isoflurane-oxygen mixture for approximately 2 minutes. The animals were transferred from the induction chamber to the 34.8-mm sample holder where anesthesia was maintained with 1.5-2% isoflurane delivered via a nose cone. Special care was taken to position the mice on their abdomen. The scanner was set to have a field of view of 20.5mm, X-ray energy of 55 kVp, Intensity of 145µA, using 1,000 projections per 360°, integration time of 200msec and reconstructed at a spatial nominal resolution of 35µm. The defect margins were aligned to a standard position, and a cylindrical volume of interest was defined (1.58mm in diameter, including partial host bone in outer periphery, and average of 35 slices in depth). A constrained 3D Gaussian filter was used to partially suppress noise in the volumes. The bone tissue was segmented by using a global thresholding procedure. Week 4 and 8 data were normalized to day 1 data obtained from the same animal to diminish variations.

Histological and immunofluorescent analyses

After sacrifice at week 8 post-surgery, the defect site including the allograft and surrounding bone tissue was explanted. Samples were fixed in in 4% formaldehyde solution, decalcified by incubation in 0.5M EDTA (pH 7.4), passed through a graded series of ethanol solutions, and embedded in paraffin. Five-micron-thick sections were cut from the paraffin blocks. Hematoxylin and eosin (H&E) staining was performed to evaluate the morphological features of the healing process, graft-to-host osseointegration, and fibrous tissue formation as previously reported [51, 52].

For immunofluorescent staining, tissues were deparaffinized, and the antigens were retrieved by incubation in Proteinase K (Agilent, Carpinteria, CA) for 20 minutes at room temperature. Nonspecific antigens were blocked by applying Normal Donkey Serum (Jackson ImmunoResearch, West Grove, PA). Slides were stained with primary antibodies, as detailed in Supplemental Table 1. The primary antibodies were applied to the slides, after which the slides were incubated at 4°C overnight and washed using PBS; the slides were then incubated with secondary antibodies for one hour at room temperature. Finally, the slides were stained with 4',6-diamidino-2-phenylindole dihydrochloride (DAPI, 300nM, Invitrogen,

Waltham, MA) for five minutes in the dark. ProLong™ Gold Antifade mounting medium (Invitrogen) was applied to the tissue. Images were captured using a Carl Zeiss Axio Imager Z1 fluorescent microscope (Carl Zeiss, Oberkochen, Germany) equipped with ApoTome and AxioCam HRc cameras. Negative controls were processed using identical protocols while omitting the primary antibody to exclude nonspecific staining. Images were captured with 4x4 tile scans at 20x objective.

Statistical analysis

All statistical analyses were performed using Prism 8 (GraphPad, La Jolla, CA); $p<0.05$ was considered statistically significant. The outcome measurements were 1) BLI intensity, 2) gene expression and 3) µCT measures. Separately for each dependent measure, 2-way analysis of variance (ANOVA) or mixed-effects analysis (BLI only), were performed using mean values with grouping of implant group; for multiple comparisons, appropriate post hoc tests were used. In figures, median (min; max) values are shown.

Results

3D printable cell-bio-ink construct maintain structure *in vitro*

The 3D printed construct (**Fig. 1B**) maintained a similar shape as our design (**Fig. 1A**). The edge of the construct is visibly thicher. The line grid is straight and visibly clear (**Fig. 1B**), and it maintained a grid pattern and clear spacing under microscopic scale (**Fig. 1C**). The line width is estimatedly 200-300 µm and the spacing between parallel lines is about 700-800 µm (**Fig. 1C**). Granual particle can be found in the SEM images (**Fig. 1C**), which are the tricalcium phosphate particles. The cross-secions of the construct is about 500 µm. The construct is thinner than the design, which could be a result of the deformation of the materials under gravity or compression. The 3D printed construct with cells (cell-bio-ink) construct also maintained a integral shape (**Fig. 1E**) as in our design (**Fig. 1A**). The addition of cells into the construct assumably changed the mechanical and rhological properties and thus we had to use a different printing parameter (30 KPa) to achieve a stable printing. And, the lines seem to be thicker and spacing to be smaller than the constructs without cells (**Fig. 1B**). The cell-bio-ink bone maintained a good shape at day 0 (**Fig. 1F**) but partly lost the integrity after 27 days culture *in vitro* (**Fig. 1G**).

Ink-Bone with both BM-MSCs and iPSC-MPCs shows increased survival and quality in vitro compared to GelXA

In the GelXa group, BLI signals were reduced between days 1 and 7. At day 14, the signal increased again. In the Ink-Bone group, the BLI signal was reduced between days 1 and 4. At day 4, the signal consistently increased until day 28. Ink-Bone resulted in a significantly higher BLI signals compared to GelXA at 28 days. No differences were observed between BM-MSCs and iNCC-MPCs (**Fig. 2A**). In the osteogenic differentiation assay using cells mixed with both bio-inks and exposed to osteogenic media, no difference in *Col 1* levels was detected between the bio-inks and cell sources (**Fig. 2B**). *ALP* levels were increased in the BM-MSC group compared to iNCC-MPC. *Oc* gene expression was increased in the Ink-Bone group compared to 2D culture and GelXA in iNCC-MPCs, and in the Ink-Bone and GelXA group versus 2D culture

in the BM-MSC group. In the GelXA group, BM-MSCs expressed higher levels of *Oc* compared to iNCC-MPCs. *On* was increased in the GelXA group compared to Ink-Bone. In each group, higher levels of *On* were measured in iNCC-MPCs compared to BM-MSCs (**Fig. 2B**).

Micro-CT analysis in vitro demonstrated no differences in the Bone Volume/Total Volume between the bio-inks. Connectivity density was increased in BM-MSCs and iNCC-MPCs and trabecular number was increased in BM-MSCs in Ink-Bone compared to GelXa (**Fig. 2C**). In both bio-inks, increased BV/TV was detected in the BM-MSC group versus bio-ink only (**Fig. 2C**). In the Ink-Bone group, BV/TV levels were increased in the BM-MSC group compared to iNCC-MPCs. In the Ink-Bone group, increased trabecular number values were measured in the BM-MSC group compared to Ink-Bone only controls (**Fig. 2C**).

Osteogenic marker expression is increased in BMP6 transfected iNCC-MPCs and BM-MSCs mixed with Ink-Bone

In response to BMP6 overexpression in Ink-Bone constructs, *Col I* was elevated compared to GFP controls. Comparing cell types, no difference between cell types was detected. *ALP* and *Oc* levels were elevated in BM-MSCs in the BMP6 group versus GFP control. No differences were detected between cell types in the GFP and BMP6 groups. *On* was increased in both BM-MSCs and iNCC-MPCs in the BMP6 group versus GFP control. Within the BMP6 group *Oc* levels were elevated in the iNCC-NPC group versus BM-MSC **(Fig. 3)**.

Addition of Ink-Bone + iNCC-MPC-BMP6 improves frontal and parietal defect healing

3D µCT image reconstruction gave an overview of the optical defect sizes of the different experimental groups at week 0, 4 and 8 post-surgery, as a result of the surgical procedure (**Fig. 4A-E**). Micro-CT analysis at week 4 demonstrated an enhanced relative bone volume ($BV_{week\ 4}$ - $BV_{week\ 0}$) in the iNCC-MPC-BMP6 group in the frontal bone compared to defect only and Ink-Bone only. At 8 weeks, the relative BV was increased in the iNCC-MPC-BMP6 as well as in the iMSC-BMP6 groups compared to defect only. No significant differences in bone volume detected between any of the other groups in the frontal bone. Except in the BM-MSC BMP-6 group, in all frontal bone groups treated with Ink-Bone, the relative bone volume was increased compared to parietal bone (**Fig. 4F**).

Increased new bone formation in frontal bone defects treated with Ink-Bone+iNCC-MPC-BMP6 observed with histological and immunofluorescent analyses

Histological evaluation performed at week 8 post-surgery demonstrated increased new bone formation and partial bridging in the iMSC-BMP6 and iNCC-MPC-BMP6 groups in the frontal bone. In the defect area, new bone formation was also detected in the BM-MSC group. However, no bone bridging between host bone and newly formed bone at the implantation site was detected. In the defect only and Ink-Bone only groups, no new bone formation was observed. In the parietal bone, new bone formation was detected in the iMSC-BMP6 and iNCC-MPC-BMP6 groups, but no integration of the newly formed bone

into the host bone tissue was observed. In the BM-MSC, Ink-Bone only and defect only groups, no or only marginal new bone was found (**Fig. 5**).

Immunofluorescent staining of the host-tissue engineered construct (Fig. 6) showed stained cell indicating survival of the implanted cells for at least 8 weeks. Expression of human Bone Sialoprotein (hBSP) and Osteonectin in the cell-bio-ink treated defects, indicates differentiation of the cells to osteoblasts, new bone tissue formation and defect repair by the implanted cells. Interestingly, the anti-hBSP antibody had a low unspecific staining in the defect treated with Bone-Ink only (Fig.6). This might indicate that some components of the Bone-ink have similarity with BSP protein.

Discussion

The results of this study show the potential of neural crest-derived progenitor cell-incorporated bio-ink to regenerate cranial defects. We demonstrated Ink-Bone to support cell survival and to promote osteogenic differentiation of iNCC-MPCs and BM-MSCs compared to GelXA in vitro. Our in vivo data demonstrates that the combination of Ink-Bone with iNCC-MPC-BMP6 stimulates cranial defect healing in the frontal bone more efficiently than BM-MSCs and iMSCs.

BLI demonstrated that both the GelXa and the Ink-Bone bio-inks supported cell viability. No difference in cell viability depending on the cell type (BM-MSC versus iNCC-MPC) was detected. Comparing bio-inks, the luciferase signal was significantly increased at day 28 in cells embedded in Ink-Bone versus GelXa. This may be a result of blending or modification of the alginate-based bio-inks, such as Ink-Bone, since this has been shown to improve molecules adhesion [53]. Comparable with our results showing an increase in BLI signals from day 4 on in the nanocellulose-alginate based Ink-Bone, an increase in cell viability between days 0–7 was demonstrated in a study using chondrocyte-incorporated nanocellulose-alginate bio-ink [54].

In the presence of osteogenic media, osteocalcin levels increased in BM-MSCs embedded in Ink-Bone and osteonectin in iNCC-MPCs embedded in GelXa, extracellular bone matrix proteins that have been shown to have synergistic effects in MSC proliferation and osteogenic differentiation [55]. Our study detected osteogenic differentiation and is in line with prior studies showing MSC differentiation in alginate-based bio-inks [13].

Micro-CT analysis of in vitro cultured bio-inks with and without cells resulted in increased BV/TV and trabecular number in the BM-MSC group and increased connectivity density in both the BM-MSC and iNCC-MPC groups compared to bio-ink only. Connectivity density and trabecular numbers were increased in the Ink-Bone group compared to GelXa group in the presence of MSCs. Micro-CT has been used since it provides a powerful platform to analyze, visualize, and explore the bio-ink scaffolds in a 3D fashion [56]. The observed increased bone formation of bio-inks combined with BM-MSCs is likely due to the strong intrinsic osteogenic potential of BM-MSCs. Multiple studies suggest that BM-MSCs are strongly involved in the process of heterotopic ossification, a process of ectopic bone tissue formation in non-bone tissues besides the potential effect of MSCs on tissue regeneration [57]. In addition to the capability of new bone

formation, bone quality is an important factor when considering a bio-ink for cranial repair. For example, in prior studies it has been shown that relatively smaller pores and a larger specific surface area assist cell attachment [58]. The increased bone volume and connectivity values in the Ink-Bone group indicate that this biomaterial is more suitable for MSC function and was therefore chosen for subsequent in vivo studies comparing the different cell types.

BMP6 transfection of BM-MSCs and iNCC-MPCs embedded in Ink-Bone resulted in an increase of the known osteogenic markers, Col1, ALP, Oc and/or On. These findings confirm the strong osteogenic potential of BMP6 that has been demonstrated by our group and others [33–35]. The osteogenic marker expression between BMP6-transfected BM-MSCs and iNCC-MPCs embedded into Ink-Bone differed depending on marker gene. However, both cell types responded to the BMP6 overexpression with osteogenic marker expression.

Our µCT data and histological analysis of the bone defects demonstrate an improved relative bone volume in frontal bone defects that were treated iNCC-MPC-BMP6 cell containing Ink-Bone at 4 weeks post-surgery. At 8 weeks, the relative BV was increased in the iNCC-MPC-BMP6 and iMSC-BMP6 groups compared to defect only, but not in the BM-MSC-BMP6 group. In a recent study by our group, the BM-MSC-Luc2-seeded allograft group showed increased BV compared to allograft only and to iNCC-MPC-Luc2-seeded allograft groups at 8 weeks post-surgery using the same mouse strain [46]. The difference in findings is likely due to several reasons: In the current study, 2mm defects in distinct areas of the frontal and parietal cranium were created, while we created 5mm defects that included part of the lambdoid and sagittal cranial sutures in the previous study. Furthermore, we transfected the cells with BMP6 in the present study and embedded the cells in Ink-Bone. Similarly, other prior studies showing an improvement of cranial defect repair using BM-MSCs applied with and without carriers created larger defects of at least 5mm in rats that included cranial sutures [59, 60]. Therefore, it is possible that stem cells present in the sutures [61], contribute to the bone regeneration in response to BM-MSC therapy in studies with larger cranial defects.

Similar to our study, Kuhn et al. demonstrated an increased bone regenerative potential of induced human embryonic stem cells on calcium phosphate cement scaffolds versus BM-MSCs in the cranium [62]. In contrast, implantation of osteoinduced iPSCs and BM-MSCs seeded on biofunctionalized macroporous calcium phosphate cement showed a similar quality of new bone during cranial regeneration [63].

Interestingly, no increase in bone regeneration was detected in the parietal bone groups that are developmentally derived from the mesoderm. Based on our findings other strategies should be considered when treating parietal bone defects. A potential treatment source may be stem cells from the cranial sutures, as these cells have shown to have a great healing potential [61].

This study is not without limitations: Due to the animal model we have chosen, the defect size we were able to create was only 2mm in diameter. While this defect was clearly large enough in size to show no bone healing in the control group (defect only), this defect size is too small to allow for addition of 3D

printed bio-ink. Larger defects in larger animal models, such as in pig, are needed allow for application of 3D printed cell containing Ink-Bone. Cranial bone healing is known to be challenging, especially in areas without cranial sutures. While our study clearly showed that combination of bio-printable bio-ink in combination with BMP6 transfected iNCC-MPCs is capable of stimulating bone regeneration, we still did not achieve full bone bridging, especially in the parietal bone. Bio-printing of the therapeutic candidate may help to overcome these challenges, since nano-topography of materials have been shown to be important for osteogenic differentiation [64].

Summary And Conclusion

The results of this study show the potential of stem cell-incorporated bio-ink to stimulate regeneration in frontal cranial defects. We demonstrated Ink-Bone to be beneficial for the survival and osteogenic differentiation of iNCC-MPCs and BM-MSCs compared to GelXA *in vitro*. The printability of bio-ink scaffolds, and their ability to support stem cell survival and osteogenic differentiation makes them attractive for craniofacial reconstruction. Our in vivo data demonstrate that combination of Ink-Bone with BMP6 overexpressing iNCC-MPC stimulates cranial defect healing in the frontal bone more efficiently than BMP6 overexpressing BM-MSCs and iMSCs. Employment of large animal models with cranial defects of 20mm minimum will allow for testing of 3D printed stem cell-embedded woven bio-ink, which may further stimulate graft-host bone integration.

Abbreviations

BM-MSC – Bone marrow mesenchymal stem cells

rhBMP - Recombinant human bone morphogenetic protein

NC – Neural crest

NCC – Neural crest cell

iPSC – Induced pluripotent stem cell

iNCC-MPC – iPSC-derived NC mesenchymal progenitor cells

Ink-Bone – CELLINK BONE

CelXA – GelXA BONE

BLI – Bioluminescent imaging

Luc2 – Luciferase2

ROI – Region of interest

Osteocalcin – Oc

Collagen type I – Col I

Alkaline phosphatase – ALP

Osteonectin – On

SQ – Subcutaneous

BV – Bone volume

TV – Total volume

H&E – Hematoxylin and eosin

DAPI – 4',6-diamidino-2-phenylindole dihydrochloride

hBSP – Human Bone Sialoprotein

Declarations

Ethics Approval and Consent to Participate

This study was approved by the Cedars-Sinai IACUC , study #IACUC007961. For iPSC derivation healthy control dermal fibroblasts from one donor were obtained from the Coriell Institute for Medical Research (Camden, NJ) and additional dermal fibroblasts and blood T-cells were derived from two healthy donors at Cedars-Sinai Medical Center.

Availability of Data and Material

The dataset(s) supporting the conclusions of this article is(are) included within the article (and its additional file(s)).

Funding

This study was supported by the NIH/NIAMS K01AR071512 to DS and by the Kosciuszko Foundation, The American Centre of Polish Culture to PN.

Authors' Contribution

Conceptualization: JDG, XB and DS;

Methodology: JDG, XB, GK, PA, PB, KS, XD, AC, CC, WJ, PN and WT;

Validation and data analysis, JDG, XB, GK, XD, AC, CC, WJ, PN, and DS;

Writing original draft: JDG, GK and DS;

Manuscript review and editing: JDG GK and DS;

Figures visualization: JDG, XB, GK, WJ, PN and DS;

Supervision: WT andDS

Funding acquisition: DS

Acknowledgments

The authors wish to acknowledge Cedars-Sinai Imaging Core facility for performing the µCT scans and Biobank and Translational Research Core for performing the histological analysis and scanning the slides.

Competing Interests

The authors have no conflict of interest.

References

1. Bhumiratana S, Vunjak-Novakovic G. Concise review: personalized human bone grafts for reconstructing head and face. Stem Cells Transl Med. 2012;1(1):64–9.
2. Elsalanty ME, Genecov DG. Bone grafts in craniofacial surgery. Craniomaxillofac Trauma Reconstr. 2009;2(3):125–34.
3. Oliver JD, Banuelos J, Abu-Ghname A, Vyas KS, Sharaf B. Alloplastic Cranioplasty Reconstruction: A Systematic Review Comparing Outcomes With Titanium Mesh, Polymethyl Methacrylate, Polyether Ether Ketone, and Norian Implants in 3591 Adult Patients. Ann Plast Surg. 2019;82(5S Suppl 4):289–94.
4. Badhey A, Kadakia S, Mourad M, Inman J, Ducic Y. Calvarial Reconstruction. Semin Plast Surg. 2017;31(4):222–6.
5. Carragee EJ, Hurwitz EL, Weiner BK. A critical review of recombinant human bone morphogenetic protein-2 trials in spinal surgery: emerging safety concerns and lessons learned. The spine journal: official journal of the North American Spine Society. 2011;11(6):471–91.
6. Salah M, Tayebi L, Moharamzadeh K, Naini FB. Three-dimensional bio-printing and bone tissue engineering: technical innovations and potential applications in maxillofacial reconstructive surgery. Maxillofac Plast Reconstr Surg. 2020;42(1):18.
7. Tian Y, Chen C, Xu X, Wang J, Hou X, Li K, Lu X, Shi H, Lee ES, Jiang HB: A Review of 3D Printing in Dentistry: Technologies, Affecting Factors, and Applications. *Scanning* 2021, 2021:9950131.
8. Murphy SV, De Coppi P, Atala A. Opportunities and challenges of translational 3D bioprinting. Nat Biomed Eng. 2020;4(4):370–80.

9. Marques CF, Diogo GS, Pina S, Oliveira JM, Silva TH, Reis RL. Collagen-based bioinks for hard tissue engineering applications: a comprehensive review. J Mater Sci Mater Med. 2019;30(3):32.
10. Pahlevanzadeh F, Mokhtari H, Bakhsheshi-Rad HR, Emadi R, Kharaziha M, Valiani A, Poursamar SA, Ismail AF, RamaKrishna S, Berto F: Recent Trends in Three-Dimensional Bioinks Based on Alginate for Biomedical Applications. *Materials (Basel)* 2020, 13(18).
11. Ahlfeld T, Guduric V, Duin S, Akkineni AR, Schutz K, Kilian D, Emmermacher J, Cubo-Mateo N, Dani S, Witzleben MV, et al. Methylcellulose - a versatile printing material that enables biofabrication of tissue equivalents with high shape fidelity. Biomater Sci. 2020;8(8):2102–10.
12. Chung JHY, Naficy S, Yue Z, Kapsa R, Quigley A, Moulton SE, Wallace GG. Bio-ink properties and printability for extrusion printing living cells. Biomater Sci. 2013;1(7):763–73.
13. Gonzalez-Fernandez T, Tenorio AJ, Campbell KT, Silva EA, Leach JK. Alginate-Based Bioinks for 3D Bioprinting and Fabrication of Anatomically Accurate Bone Grafts. Tissue Eng Part A. 2021;27(17–18):1168–81.
14. Pittenger MF, Mackay AM, Beck SC, Jaiswal RK, Douglas R, Mosca JD, Moorman MA, Simonetti DW, Craig S, Marshak DR. Multilineage potential of adult human mesenchymal stem cells. Science. 1999;284(5411):143–7.
15. Long T, Zhu Z, Awad HA, Schwarz EM, Hilton MJ, Dong Y. The effect of mesenchymal stem cell sheets on structural allograft healing of critical sized femoral defects in mice. Biomaterials. 2014;35(9):2752–9.
16. Hoffman MD, Xie C, Zhang X, Benoit DS. The effect of mesenchymal stem cells delivered via hydrogel-based tissue engineered periosteum on bone allograft healing. Biomaterials. 2013;34(35):8887–98.
17. Chang SC, Chung HY, Tai CL, Chen PK, Lin TM, Jeng LB. Repair of large cranial defects by hBMP-2 expressing bone marrow stromal cells: comparison between alginate and collagen type I systems. J biomedical Mater Res Part A. 2010;94(2):433–41.
18. Zhao H, Feng J, Ho TV, Grimes W, Urata M, Chai Y. The suture provides a niche for mesenchymal stem cells of craniofacial bones. Nat Cell Biol. 2015;17(4):386–96.
19. Li S, Quarto N, Senarath-Yapa K, Grey N, Bai X, Longaker MT. Enhanced Activation of Canonical Wnt Signaling Confers Mesoderm-Derived Parietal Bone with Similar Osteogenic and Skeletal Healing Capacity to Neural Crest-Derived Frontal Bone. PLoS ONE. 2015;10(10):e0138059.
20. Jiang X, Iseki S, Maxson RE, Sucov HM, Morriss-Kay GM. Tissue origins and interactions in the mammalian skull vault. Dev Biol. 2002;241(1):106–16.
21. Senarath-Yapa K, Li S, Meyer NP, Longaker MT, Quarto N. Integration of multiple signaling pathways determines differences in the osteogenic potential and tissue regeneration of neural crest-derived and mesoderm-derived calvarial bones. Int J Mol Sci. 2013;14(3):5978–97.
22. Quarto N, Wan DC, Kwan MD, Panetta NJ, Li S, Longaker MT. Origin matters: differences in embryonic tissue origin and Wnt signaling determine the osteogenic potential and healing capacity of frontal and parietal calvarial bones. J Bone Miner Res. 2010;25(7):1680–94.

23. Li S, Meyer NP, Quarto N, Longaker MT. Integration of multiple signaling regulates through apoptosis the differential osteogenic potential of neural crest-derived and mesoderm-derived Osteoblasts. PLoS ONE. 2013;8(3):e58610.
24. Li S, Quarto N, Longaker MT. Activation of FGF signaling mediates proliferative and osteogenic differences between neural crest derived frontal and mesoderm parietal derived bone. PLoS ONE. 2010;5(11):e14033.
25. Achilleos A, Trainor PA. Neural crest stem cells: discovery, properties and potential for therapy. Cell Res. 2012;22(2):288–304.
26. Morikawa S, Ouchi T, Shibata S, Fujimura T, Kawana H, Okano H, Nakagawa T: Applications of Mesenchymal Stem Cells and Neural Crest Cells in Craniofacial Skeletal Research. *Stem cells international* 2016, 2016:2849879.
27. Takahashi K, Yamanaka S. Induction of pluripotent stem cells from mouse embryonic and adult fibroblast cultures by defined factors. Cell. 2006;126(4):663–76.
28. Menendez L, Yatskievych TA, Antin PB, Dalton S. Wnt signaling and a Smad pathway blockade direct the differentiation of human pluripotent stem cells to multipotent neural crest cells. Proc Natl Acad Sci U S A. 2011;108(48):19240–5.
29. Muhammad A, Kim K, Epifantseva I, Aghamaleky-Sarvestany A, Simpkinson ME, Carmona S, Landeros J, Bell S, Svaren J, Baloh RH. Cell transplantation strategies for acquired and inherited disorders of peripheral myelin. Ann Clin Transl Neurol. 2018;5(2):186–200.
30. Glaeser JD, Behrens P, Stefanovic T, Salehi K, Papalamprou A, Tawackoli W, Metzger MF, Eberlein S, Nelson T, Arabi Y, et al: Neural crest-derived mesenchymal progenitor cells enhance cranial allograft integration. *Stem cells translational medicine* 2021.
31. Gautschi OP, Frey SP, Zellweger R. Bone morphogenetic proteins in clinical applications. ANZ J Surg. 2007;77(8):626–31.
32. Kang Q, Sun MH, Cheng H, Peng Y, Montag AG, Deyrup AT, Jiang W, Luu HH, Luo J, Szatkowski JP, et al. Characterization of the distinct orthotopic bone-forming activity of 14 BMPs using recombinant adenovirus-mediated gene delivery. Gene Ther. 2004;11(17):1312–20.
33. Cheng H, Jiang W, Phillips FM, Haydon RC, Peng Y, Zhou L, Luu HH, An N, Breyer B, Vanichakarn P, et al. Osteogenic activity of the fourteen types of human bone morphogenetic proteins (BMPs). J Bone Joint Surg Am. 2003;85-A(8):1544–52.
34. Luu HH, Song WX, Luo X, Manning D, Luo J, Deng ZL, Sharff KA, Montag AG, Haydon RC, He TC. Distinct roles of bone morphogenetic proteins in osteogenic differentiation of mesenchymal stem cells. J Orthop Res. 2007;25(5):665–77.
35. Mizrahi O, Sheyn D, Tawackoli W, Kallai I, Oh A, Su S, Da X, Zarrini P, Cook-Wiens G, Gazit D, et al. BMP-6 is more efficient in bone formation than BMP-2 when overexpressed in mesenchymal stem cells. Gene Ther. 2013;20(4):370–7.
36. Gnecchi M, Melo LG. Bone marrow-derived mesenchymal stem cells: isolation, expansion, characterization, viral transduction, and production of conditioned medium. Methods Mol Biol.

2009;482:281–94.

37. Sheyn D, Ben-David S, Shapiro G, De Mel S, Bez M, Ornelas L, Sahabian A, Sareen D, Da X, Pelled G, et al. Human Induced Pluripotent Stem Cells Differentiate Into Functional Mesenchymal Stem Cells and Repair Bone Defects. Stem cells translational medicine. 2016;5(11):1447–60.
38. Sheyn D, Kallai I, Tawackoli W, Cohn Yakubovich D, Oh A, Su S, Da X, Lavi A, Kimelman-Bleich N, Zilberman Y, et al. Gene-modified adult stem cells regenerate vertebral bone defect in a rat model. Mol Pharm. 2011;8(5):1592–601.
39. Kimelman NB, Kallai I, Sheyn D, Tawackoli W, Gazit Z, Pelled G, Gazit D. Real-time bioluminescence functional imaging for monitoring tissue formation and regeneration. Methods Mol Biol. 2013;1048:181–93.
40. Kimelman-Bleich N, Pelled G, Zilberman Y, Kallai I, Mizrahi O, Tawackoli W, Gazit Z, Gazit D. Targeted gene-and-host progenitor cell therapy for nonunion bone fracture repair. Mol Ther. 2011;19(1):53–9.
41. Sheyn D, Cohn-Yakubovich D, Ben-David S, De Mel S, Chan V, Hinojosa C, Wen N, Hamilton GA, Gazit D, Gazit Z. Bone-chip system to monitor osteogenic differentiation using optical imaging. Microfluid Nanofluidics 2019, 23(8).
42. Sheyn D, Pelled G, Netanely D, Domany E, Gazit D. The effect of simulated microgravity on human mesenchymal stem cells cultured in an osteogenic differentiation system: a bioinformatics study. Tissue Eng Part A. 2010;16(11):3403–12.
43. Sheyn D, Pelled G, Zilberman Y, Talasazan F, Frank JM, Gazit D, Gazit Z. Nonvirally engineered porcine adipose tissue-derived stem cells: use in posterior spinal fusion. Stem Cells. 2008;26(4):1056–64.
44. Glaeser JD, Salehi K, Kanim LE, Ju DG, Hyuk Yang J, Behrens PH, Eberlein SA, Metzger MF, Arabi Y, Stefanovic T, et al: Electrospun, synthetic bone void filler promotes human MSC function and BMP-2 mediated spinal fusion. J Biomater Appl 2020:885328220937999.
45. Glaeser JD, Salehi K, Kanim LEA, Sheyn D, NaPier Z, Behrens PH, Garcia L, Cuellar JM, Bae HW. Anti-Inflammatory Peptide Attenuates Edema and Promotes BMP-2-Induced Bone Formation in Spine Fusion. Tissue Eng Part A. 2018;24(21–22):1641–51.
46. Glaeser JD, Behrens P, Stefanovic T, Salehi K, Papalamprou A, Tawackoli W, Metzger MF, Eberlein S, Nelson T, Arabi Y, et al. Neural crest-derived mesenchymal progenitor cells enhance cranial allograft integration. Stem Cells Transl Med. 2021;10(5):797–809.
47. Kallai I, Mizrahi O, Tawackoli W, Gazit Z, Pelled G, Gazit D. Microcomputed tomography-based structural analysis of various bone tissue regeneration models. Nat Protoc. 2011;6(1):105–10.
48. Sheyn D, Kallai I, Tawackoli W, Cohn Yakubovich D, Oh A, Su S, Da X, Lavi A, Kimelman-Bleich N, Zilberman Y, et al. Gene-modified adult stem cells regenerate vertebral bone defect in a rat model. Mol Pharm. 2011;8(5):1592–601.
49. Sheyn D, Cohn Yakubovich D, Kallai I, Su S, Da X, Pelled G, Tawackoli W, Cook-Weins G, Schwarz EM, Gazit D, et al. PTH promotes allograft integration in a calvarial bone defect. Mol Pharm. 2013;10(12):4462–71.

50. Reynolds DG, Shaikh S, Papuga MO, Lerner AL, O'Keefe RJ, Schwarz EM, Awad HA. muCT-based measurement of cortical bone graft-to-host union. J bone mineral research: official J Am Soc Bone Mineral Res. 2009;24(5):899–907.
51. Sheyn D, Kimelman-Bleich N, Pelled G, Zilberman Y, Gazit D, Gazit Z. Ultrasound-based nonviral gene delivery induces bone formation in vivo. Gene Ther. 2008;15(4):257–66.
52. Sheyn D, Kallai I, Tawackoli W, Cohn Yakubovich D, Oh A, Su S, Da X, Lavi A, Kimelman-Bleich N, Zilberman Y, et al: Gene-Modified Adult Stem Cells Regenerate Vertebral Bone Defect in a Rat Model. Mol Pharm 2011.
53. Panwar A, Tan LP. Current Status of Bioinks for Micro-Extrusion-Based 3D Bioprinting. Molecules 2016, 21(6).
54. Markstedt K, Mantas A, Tournier I, Martinez Avila H, Hagg D, Gatenholm P. 3D Bioprinting Human Chondrocytes with Nanocellulose-Alginate Bioink for Cartilage Tissue Engineering Applications. Biomacromolecules. 2015;16(5):1489–96.
55. Carvalho MS, Cabral JM, da Silva CL, Vashishth D. Synergistic effect of extracellularly supplemented osteopontin and osteocalcin on stem cell proliferation, osteogenic differentiation, and angiogenic properties. J Cell Biochem. 2019;120(4):6555–69.
56. Cengiz IF, Oliveira JM, Reis RL. Micro-CT - a digital 3D microstructural voyage into scaffolds: a systematic review of the reported methods and results. Biomater Res. 2018;22:26.
57. Kan C, Chen L, Hu Y, Lu H, Li Y, Kessler JA, Kan L. Microenvironmental factors that regulate mesenchymal stem cells: lessons learned from the study of heterotopic ossification. Histol Histopathol. 2017;32(10):977–85.
58. O'Brien FJ, Harley BA, Yannas IV, Gibson LJ. The effect of pore size on cell adhesion in collagen-GAG scaffolds. Biomaterials. 2005;26(4):433–41.
59. Al-Hezaimi K, Ramalingam S, Al-Askar M, ArRejaie AS, Nooh N, Jawad F, Aldahmash A, Atteya M, Wang CY. Real-time-guided bone regeneration around standardized critical size calvarial defects using bone marrow-derived mesenchymal stem cells and collagen membrane with and without using tricalcium phosphate: an in vivo micro-computed tomographic and histologic experiment in rats. Int J Oral Sci. 2016;8(1):7–15.
60. Freitas GP, Lopes HB, Souza ATP, Oliveira P, Almeida ALG, Souza LEB, Coelho PG, Beloti MM, Rosa AL. Cell Therapy: Effect of Locally Injected Mesenchymal Stromal Cells Derived from Bone Marrow or Adipose Tissue on Bone Regeneration of Rat Calvarial Defects. Sci Rep. 2019;9(1):13476.
61. Park S, Zhao H, Urata M, Chai Y. Sutures Possess Strong Regenerative Capacity for Calvarial Bone Injury. Stem Cells Dev. 2016;25(23):1801–7.
62. Kuhn LT, Liu Y, Boyd NL, Dennis JE, Jiang X, Xin X, Charles LF, Wang L, Aguila HL, Rowe DW, et al. Developmental-like bone regeneration by human embryonic stem cell-derived mesenchymal cells. Tissue Eng Part A. 2014;20(1–2):365–77.
63. Wang P, Liu X, Zhao L, Weir MD, Sun J, Chen W, Man Y, Xu HH. Bone tissue engineering via human induced pluripotent, umbilical cord and bone marrow mesenchymal stem cells in rat cranium. Acta

Biomater. 2015;18:236–48.

64. Zhu GY, Liu YH, Liu W, Huang XQ, Zhang B, Zheng ZL, Wei X, Xu JZ, Zhao ZH. Surface Epitaxial Nano-Topography Facilitates Biomineralization to Promote Osteogenic Differentiation and Osteogenesis. ACS Omega. 2021;6(33):21792–800.

Figures

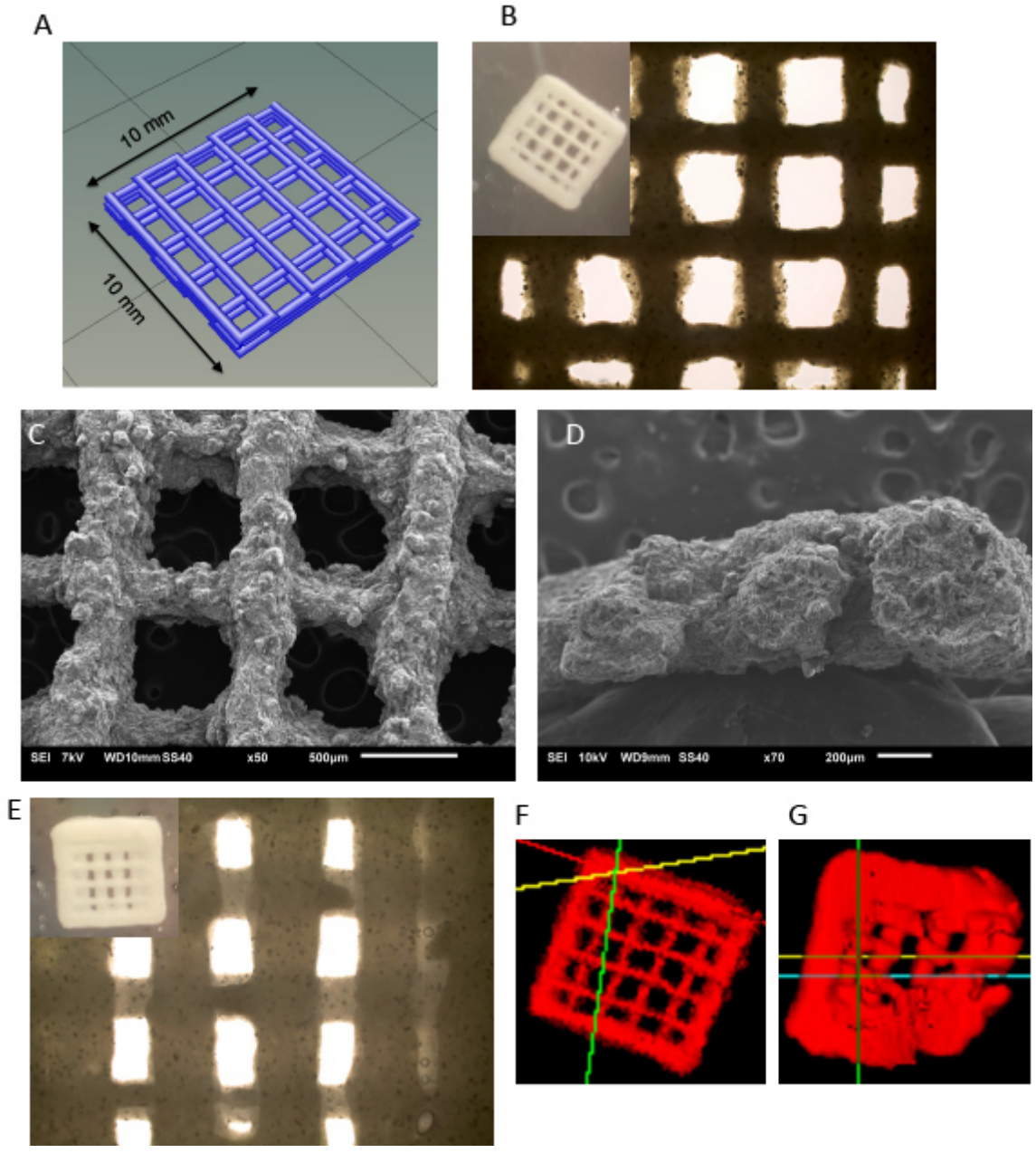

Figure 1

3D printed constructs for bone regeneration. 3D printed scaffold can be designed and printed with or without cells. (A) Design of 3D printed scaffolds. (B-D) Characterization of 3D printed scaffolds. (B) optical image, (C) SEM from top view, and (D) SEM from cross-section of 3D printed scaffold without

cells. (E) optical image of 3D printed scaffold with cells (9m/ml). The uCT images of 3D printed scaffolds (F) without cells and (G) with 9m/ml cells and cultured after 27 days. In (A), the scaffold design is 10 mm * 10 mm * 2 mm square. Printed at 10mm/s. Air pressure is 25kpa for (B) and (F), and 30kpa for (C-E) and (G). The original magnifications for (C) and (D) are x50 and x70 respectively.

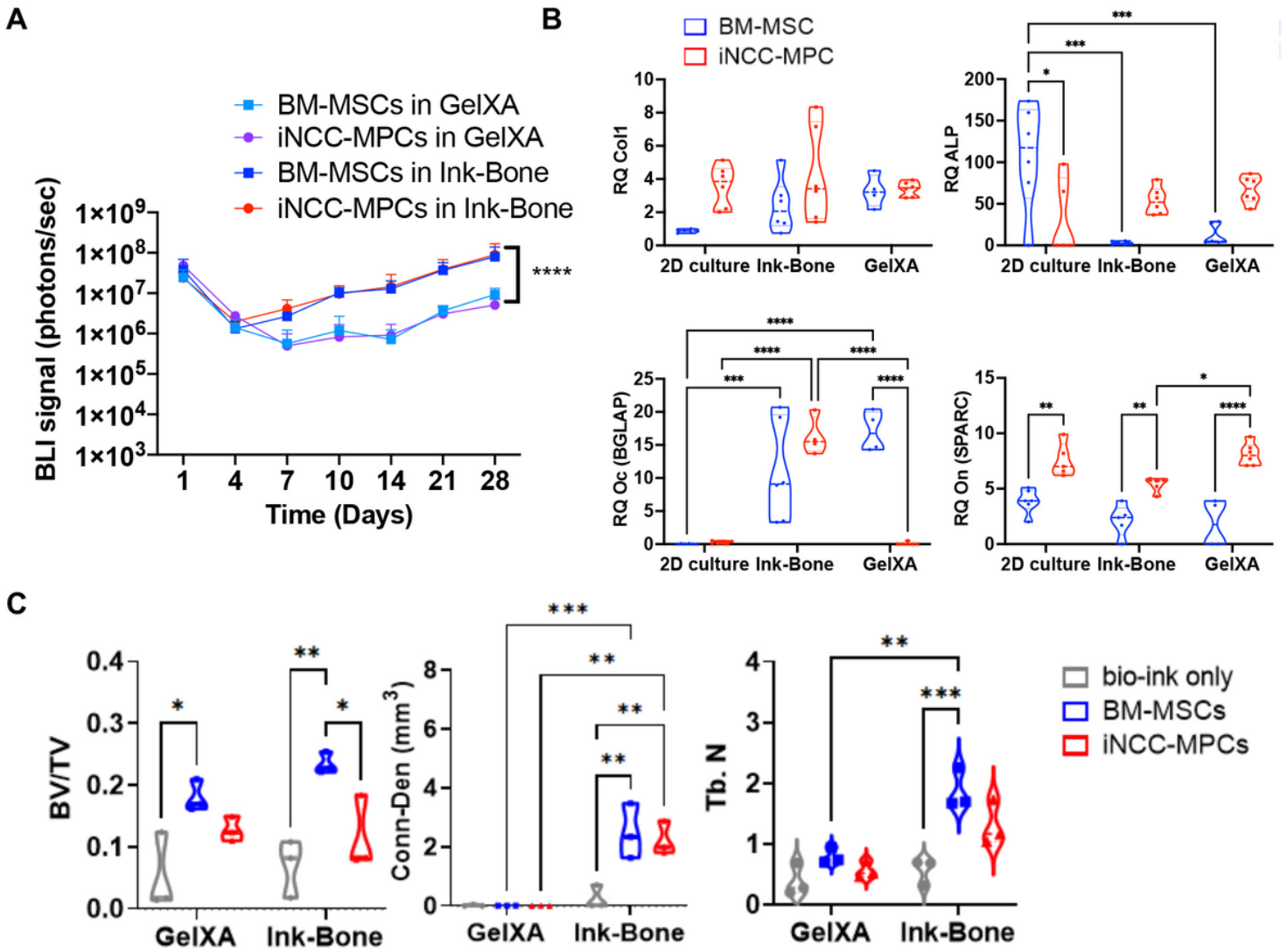

Figure 2

Cell viability and in vitro bone formation increased in Ink-bone group. A. Cells were labeled with a Luciferase reporter gene and their viability in the two bio inks was assessed by BLI in vitro. n≥4. **B.** Cells were cultured in 2D or in bio-ink 3D constructs in osteogenic media. Osteogenic gene expression was tested on Day 10. n≥4. **C.** In vitro bone formation of cells in the bio-inks was evaluated using μCT at 3 weeks and compared to Ink-Bone only. n=3. $^{*}p<0.05$, $^{**}p<0.01$, $^{***}p<0.001$, $^{****}p<0.0001$.

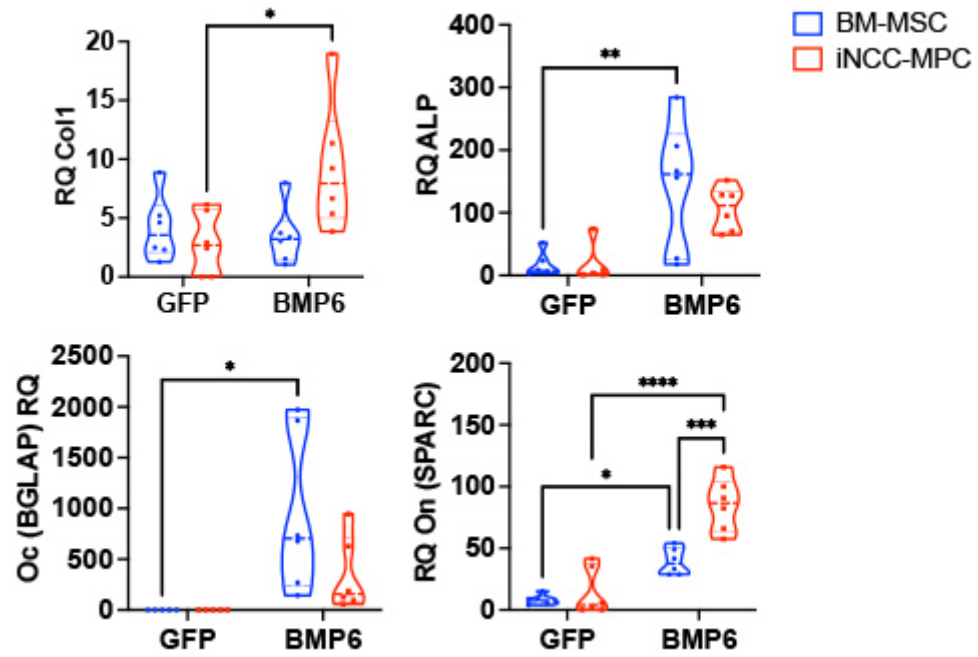

Figure 3

Osteogenesis marker expression increases in BMP6 transfected cells in Ink-Bone. A. Cells were cultured in 2D or in bio-ink 3D constructs in osteogenic media. Osteogenic gene expression was tested on Day 10. **B.** Gene expression of cells transfected with BMP6 and cultured in Ink-Bone constructs for 10 days. *p<0.05, **p<0.01, ***p<0.001, ****p<0.0001, n³5.

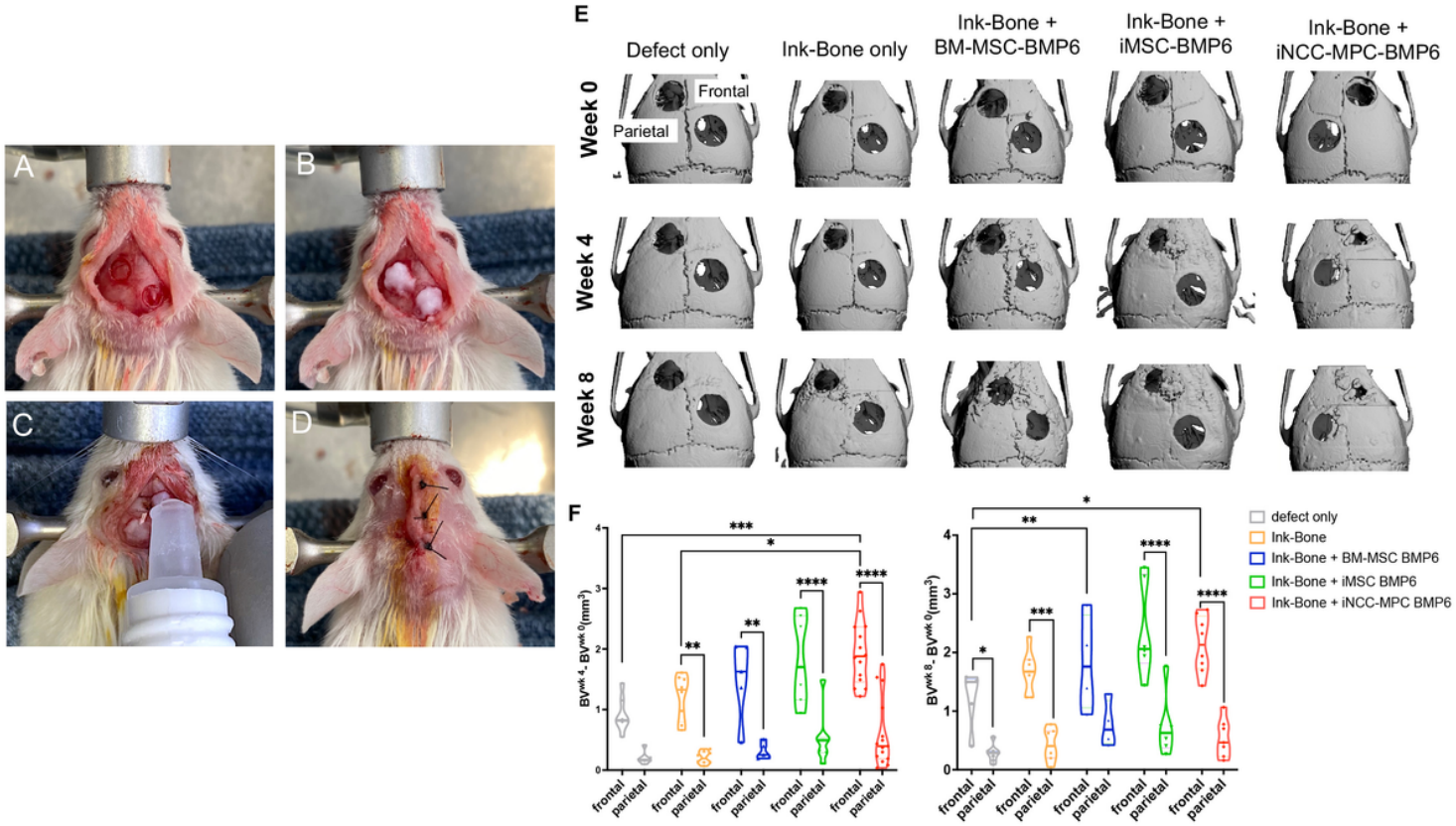

Figure 4

Cranial defect filling with Ink-Bone seeded with iNCC-MPC-BMP6 results in increased bone volume in the frontal bone. A. Surgical approach to create calvarial defects in the frontal and parietal bone. Shown is the fixated cranium with circular defects in the frontal and parietal bone. **B.** Filling of the defects with Ink-Bone. **C.** Crosslinking of Ink-Bone using $CaCl_2$ solution. **D.** The sutured skin. **E.** 3D reconstruction of the cranial defects treated with Ink-Bone with and without cells or untreated at weeks 0 and 4. **F.** Violin plots showing the change in bone volume in the different experimental groups and implantation sites between weeks 0 and 4, and 0 and 8. * p<0.05, ** p<0.01, ***p<0.001, ****p<0.0001, n³5.

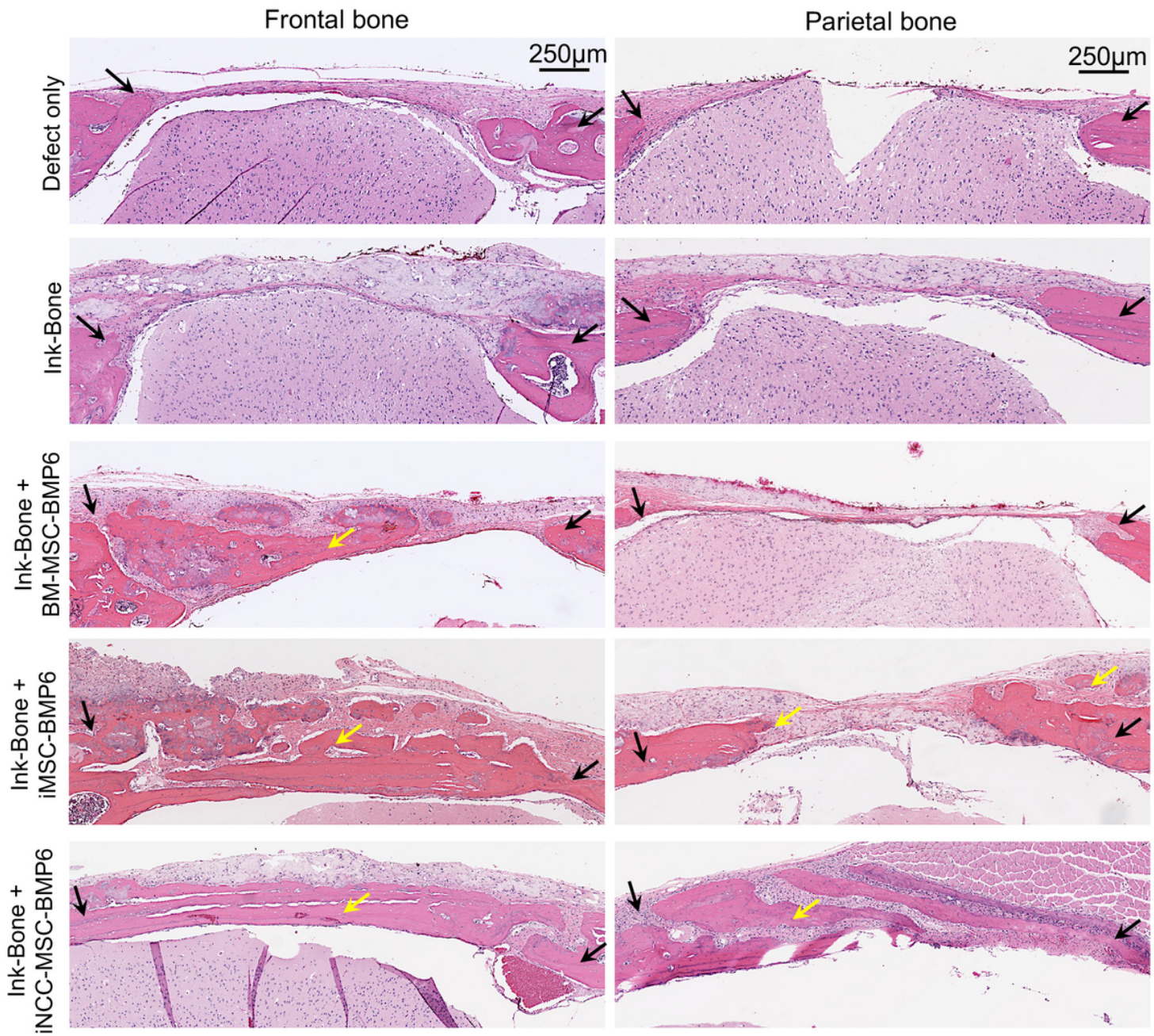

Figure 5

Histological evaluation at week 8 demonstrates increased new bone formation in frontal bone defects treated with Ink-Bone+iNCC-MPC-BMP6. Shown is the H&E staining of the frontal bone defects treated with the different experimental groups. Black arrows: edges of defect site, yellow arrow: new bone formation.

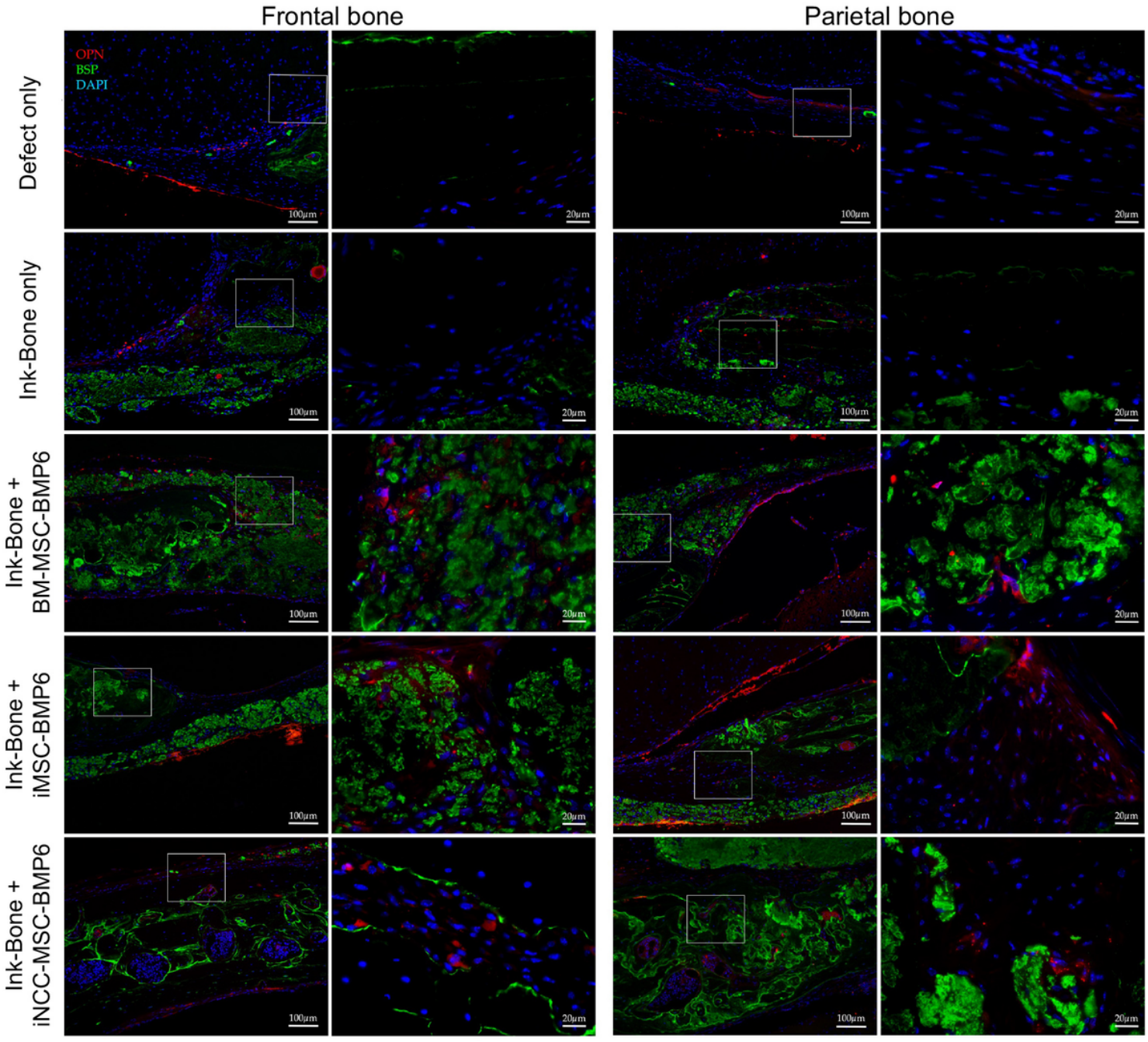

Figure 6

Immunofluorescence staining of the calvarial defect repair in a mouse model using Ink-Bone + iNCC-MPC-BMP6 and control groups. Immunofluorescence shows a DAPI, anti-human OPN (osteonectin) or human BSP (bone sialoprotein) staining. The antibody against BSP Scale bars indicate 100μm in the left and 20μm in magnified images in the right columns.

Supplementary Files

This is a list of supplementary files associated with this preprint. Click to download.

- Abstract.jpg
- CranialinkSupplement14.10.2022GK.docx